Article:
Jie, Z., Berto, F. and Susmel, L. (2020) Fatigue behaviour of pitted/cracked high-strength steel wires based on the SED approach. International Journal of Fatigue, 135. 105564. ISSN: 0142-1123

https://doi.org/10.1016/j.ijfatigue.2020.105564

Fatigue behaviour of pitted/cracked high-strength steel wires based on the SED approach

Zhiyu Jie[1], Filippo Berto[2], Luca Susmel[3]

[1]Department of Civil Engineering, Ningbo University, Ningbo 315211, China

[2]Norwegian University of Science and Technology, NO-7491Trondheim, Norway

[3]Department of Civil and Structural Engineering, The University of Sheffield, Sheffield S1 3JD, UK

Abstract

The accuracy of the Strain Energy Density (SED) approach in assessing fatigue strength of corroded metallic wires was checked against a large number of literatue data generated by testing pitted/cracked high-strength steel cables. These experimental results were re-analysed by determining the averaged SED ranges both analytically and numerically. A value of the SED critical radius of 0.06mm was used to determine a reference scatter band suitable for assessing fatigue damage in pitted/cracked wires. The SED approach was seen to result in a level of accuracy higher than the one obtained by applying the classic nominal stress based approach.

Keywords: fatigue strength; high-strength steel wires; Notch Stress Intensity Factor; Strain Energy Density; critical radius.

Nomenclature

a, b	depth and half-width of semi-elliptical cracks
d, l, w	depth, length and width of corrosion pits
D	wire diameter
e_1, e_2	shape functions
k	negative inverse slope
K_1, K_2	Mode I and Mode II N-SIFs
N_f	experimental number of cycles to failure
$N_{f,e}$	estimated number of cycles to failure
N_A	reference number of cycles to failure
P_S	probability of survival
r, θ	local polar coordinates
r_o	distance between notch tip and centre of the reference volume
R	load ratio
R_o	radius of the control volume
T_σ, $T_{\Delta K}$, $T_{\Delta \overline{W}}$	scatter ratio of the endurance limit for 90% and 10% probabilities of survival
V	total control volume
W	strain energy density
$\overline{W}$	averaged strain energy density
$\sigma_{\theta\theta}$, σ_{rr}, $\tau_{r\theta}$	stress components
λ_1, λ_2	Williams' eigenvalues depending on the notch opening angle
2α	notch opening angle
χ_1, χ_2	auxiliary parameters depending on the notch opening angle
σ_{11}, σ_{22}, σ_{33}, σ_{12}	stress components
ν	Poisson's ratio
ΔK_1	Mode I N-SIF range
$\Delta K_{1,A}$	reference value of Mode I N-SIF range at N_A cycles to failure
ΔK_{th}	range of the threshold value of the stress intensity factor
$\Delta \overline{W}$	averaged SED range
$\Delta \overline{W}_{Fi}$	strain energy density rane for the *i*-th finite element
$\Delta \overline{W}_{notch}$	SED range for notched material
$\Delta \overline{W}_{plain}$	SED range for plain material
$\Delta\sigma_A$	plain material endurance limit range at N_A cycles to failure
$\Delta\sigma_{nom}$	gross nominal stress range
$\widetilde{\omega}_1$, F, H, I_1	functions of 2α, ν and R_o
Ω	area of control volume
ρ	notch root radius
σ_{max}	maximum principal stress

1. Introduction

Thanks to their excellent tensile properties, high-strength steel wires are widely used in cable-stayed bridges as main load-carrying components. Unfortunately, during in-service operations and, in particular, under cyclic loading due to traffic, metallic wires can break due to fatigue. In this context, the long-term durability issue is complicated by the fact that the environment as well plays a role of primary importance. In particular, the presence of aggressive ambient conditions leads, over time, to uniform and localised corrosion, with the resulting superficial discontinuities (e.g. pits and cracks) markedly shortening the fatigue life of steel wires due to localised stress concentration phenomena [1].

As far as corrosion pits are concerned, in-service metallic cables are seen to be weakened by superficial cavities with different shapes [2]. Accordingly, when it comes to modelling pits explicitly, they are usually schematised either as hemispherical notches [3, 4], as semi-ellipsoidal notches [5, 6], or as cavities with bullet shape [7, 8]. These different assumptions about the pit profile allow the resulting local stress concentration phenomena to be quantified accurately, with this holding true provided that the relevant dimensions of the pits under investigation are determined with an adequate level of accuracy [9].

Turning to the stress concentration effect in fatigue, the problem of assessing the strength of notched components under cyclic loading has been investigated widely since the beginning of the last century. However, in spite of the large amount of both theoretical and experimental work that has been done since the initial pioneering studies in the field, this research topic is still very popular due to its impact on mechanical applications of practical interest.

As far as notches are concerned, examination of the state of the art shows that several approaches have been developed during the years to assess the fatigue strength of structural members. Amongst those design methodologies that have been devised and validated experimentally, certainly the Theory of Critical Distances (TCD) [10, 11], the Notch-Stress Intensity Factor (N-SIF) approach [12, 13], the Strain Energy Density (SED) method [14, 15], and the Peak Stress Method [16, 17] deserve to be mentioned explicitly.

If attention is specifically focussed on the SED approach, certainly its most remarkable feature is that this notch fatigue assessment technique can be applied by directly post-processing the results from conventional linear-elastic Finite Element (FE) models, with these models being made using a coarse mesh in the highly-stressed regions [18, 19] which gives substantial advantages in 3D complex models.

While in recent years the SED method has been used successfully to address a variety of static/fatigue assessment problems involving stress concentrators of different kind, so far it has never been attempted to be applied to model and quantify fatigue damage in pitted/cracked high-strength steel wires which is still an open challenging issue worth to be deeply investigated. Therefore, extending the use of the SED approach to the fatigue assessment of corroded steel cables represents the ultimate goal of the research work discussed in the following sections.

2. Fundamentals of the Strain Energy Density approach

The SED approach takes as a starting point the assumption that failure takes place as soon as the SED averaged in a control volume reaches a critical value, with such a critical value being treated as a material property.

In the presence of a sharp notch (Fig. 1), the stress components in the stress concentration region can be used to determine the Mode I and Mode II N-SIFs according to the following standard definitions [12, 13]:

$$K_1 = \sqrt{2\pi} \lim_{r\to 0^+} r^{1-\lambda_1} \sigma_{\theta\theta}(r, \theta = 0) \quad (1)$$

$$K_2 = \sqrt{2\pi} \lim_{r\to 0^+} r^{1-\lambda_2} \tau_{r\theta}(r, \theta = 0) \quad (2)$$

In Eqs (1) and (2) r and θ are the local polar coordinate, $\sigma_{\theta\theta}$ and $\tau_{r\theta}$ are the stress components, λ_1 and λ_2 are Williams' eigenvalues depending on the notch opening angle 2α (see Tab. 1), and K_1 and K_2 are the Mode I and Mode II N-SIFs, respectively.

The stress distribution for a sharp V-notch under Mode I loading can be written as [20]:

$$\begin{Bmatrix}\sigma_{\theta\theta}\\ \sigma_{rr}\\ \tau_{r\theta}\end{Bmatrix}=\frac{1}{\sqrt{2\pi}}\frac{r^{\lambda_1-1}K_1}{(1+\lambda_1)+\chi_1(1-\lambda_1)}\left[\begin{Bmatrix}(1+\lambda_1)\cos(1-\lambda_1)\theta\\ (3-\lambda_1)\cos(1-\lambda_1)\theta\\ (1-\lambda_1)\sin(1-\lambda_1)\theta\end{Bmatrix}+\chi_1(1-\lambda_1)\begin{Bmatrix}\cos(1+\lambda_1)\theta\\ -\cos(1+\lambda_1)\theta\\ \sin(1+\lambda_1)\theta\end{Bmatrix}\right] \quad (3)$$

and the stress distribution under Mode II as:

$$\begin{Bmatrix}\sigma_{\theta\theta}\\ \sigma_{rr}\\ \tau_{r\theta}\end{Bmatrix}=\frac{1}{\sqrt{2\pi}}\frac{r^{\lambda_2-1}K_2}{(1-\lambda_2)+\chi_2(1+\lambda_2)}\left[\begin{Bmatrix}-(1+\lambda_2)\sin(1-\lambda_2)\theta\\ -(3-\lambda_2)\sin(1-\lambda_2)\theta\\ (1-\lambda_2)\cos(1-\lambda_2)\theta\end{Bmatrix}+\chi_2(1+\lambda_2)\begin{Bmatrix}-\sin(1+\lambda_2)\theta\\ \sin(1+\lambda_2)\theta\\ \cos(1+\lambda_2)\theta\end{Bmatrix}\right] \quad (4)$$

where auxiliary parameters χ_1 and χ_2 depend on the notch opening angle (refer to Ref. [13] for the analytical determination of these parameters).

The total elastic SED for an isotropic material can be expressed in the following form [21]:

$$W=\frac{1}{2E}[\sigma_{11}^2+\sigma_{22}^2+\sigma_{33}^2-2\nu(\sigma_{11}\sigma_{22}+\sigma_{11}\sigma_{33}+\sigma_{22}\sigma_{33})-2(1+\nu)\sigma_{12}^2] \quad (5)$$

where σ_{11}, σ_{22}, σ_{33} and σ_{12} are the relevant stress components at the point of interest and W is the total SED calculated by including both the deviatoric and volumetric contributions. Thus, by taking full advantage of the N-SIFs as defined above, the averaged SED in a control volume in the vicinity of the tip of a sharp notch can be calculated as follows (Fig. 2) [22]:

$$\bar{W}=\frac{1}{E}\left[e_1\cdot\frac{K_1^2}{R_0^{2(1-\lambda_1)}}+e_2\cdot\frac{K_2^2}{R_0^{2(1-\lambda_2)}}\right] \quad (6)$$

where R_0 is the radius of the control volume, whereas e_1 and e_2 are two shape functions that depend on the notch opening angle, 2α, as well as on Poisson's ratio, ν. In particular, for ν=0.3, functions e_1 and e_2 take on the following form [22]:

$$e_1 = -5.373 \cdot 10^{-6}(2\alpha)^2 + 6.151 \cdot 10^{-4}(2\alpha) + 0.1330 \quad (7)$$

$$e_2 = 4.809 \cdot 10^{-6}(2\alpha)^2 - 2.346 \cdot 10^{-4}(2\alpha) + 0.3400 \quad (8)$$

Under pure Mode I fatigue loading, the control radius R_0 needed to apply the SED approach can directly be obtained by using the following expression [19]:

$$R_0 = \left(\frac{\sqrt{2e_1}\cdot\Delta K_{1A}}{\Delta\sigma_A}\right)^{\frac{1}{1-\lambda_1}} \quad (9)$$

where ΔK_{1A} is the reference value of the N-SIF range of the severely notched material and $\Delta\sigma_A$ is the plain material endurance limit, with these two fatigue design quantities being usually extrapolated at a reference number of cycles to failure, N_A, either equal to $2{\cdot}10^6$ or to $5{\cdot}10^6$. In those circumstances where ΔK_{1A} is not directly available, given the material, control radius R_0 can also be defined via the SED determined by testing a series of specimens containing a known sharp geometrical feature, i.e. [23]:

$$\Delta\bar{W}_{plain} = \Delta\bar{W}_{notch}(R_0) \quad (10)$$

where $\Delta\bar{W}_{plain}$ and $\Delta\bar{W}_{notch}(R_0)$ are the SED ranges at N_A cycles to failure from the plain and the notched samples, respectively. In Eq. (10) the un-known variable is the control radius, R_0, and it can easily be determined by using a standard recursive optimisation method.

Turning to blunt notches (Fig. 3), the averaged SED, $\bar{W}$, in the vicinity of the tip of a notch having a root radius larger than zero can directly be determined according to the following relationship [24]:

$$\bar{W} = \left(\frac{I_1}{2\Omega}\right) r_0^{2(1-\lambda_1)} \left[\frac{\sqrt{2\pi}}{1+\tilde{\omega}_1}\right]^2 \frac{\sigma_{max}^2}{E} = F(2\alpha)H\left(2\alpha, \frac{R_0}{\rho}\right)\frac{\sigma_{max}^2}{E} \quad (11)$$

where

$$F(2\alpha) = \left(\frac{q-1}{q}\right)^{2(1-\lambda_1)} \left[\frac{\sqrt{2\pi}}{1+\widetilde{\omega}_1}\right]^2 \quad (12)$$

In Eqs (11) and (12) the meaning of the symbols being used is as follows [24]: parameters $\widetilde{\omega}_1$ and $F(2\alpha)$ depend on the notch opening angle (see Tab. 2); H varies with the notch opening angle and Poisson's ratio; Ω is the area of control volume; σ_{max} is the maximum principal stress; r_o is the distance between the notch tip and the centre of the control volume (Fig. 3), I1 is a function of the notch opening angle, Poisson's ratio, and the control radius and, finally, ρ is the notch radius. Eq. (11) can be used also under in-plane mixed Mode I/II loading by using the local Mode I concept [22].

Since the different geometrical parameters used in Eqs (11) and (12) depend on the geometry of the stress raiser being assessed [24], it is worth concluding the present section by recalling that, according to Ref. [25], the opening angle for elliptical notches can be determined using the following equation:

$$2\alpha = 192.64\left(1 + 4\frac{d}{l}\right)^{-0.916} \quad (13)$$

where *d* is the depth, and *l* is the width of the notch.

3. Experimental results and Finite Element modelling

In order to investigate the accuracy of the SED approach in estimating the fatigue strength of metallic wires containing geometrical defects, a large number of experimental results were

taken from the technical literature. The test data being collected by performing this systematic data-mining exercise are listed in Tables 3 to 5 [26-33].

According to Fig. 4, the defects characterising the wire specimens used to generate the results reported in the above tables were modelled by considering two types of finite radius stress concentrators, i.e. (i) hemispherical and semi-elliptical corrosion pits and (ii) semi-elliptical cracks [26-33]. In the present study, as far corrosion pits are concerned (Figs 4a and 4b), depth is denoted as d, length as l and width as w. Pit length l and width w are assumed to be parallel and perpendicular to the loading direction, respectively. Turning to the semi-elliptical cracks, according to Fig. 4c, the depth is denoted as a and the half-width as b.

The linear-elastic stress distribution in the vicinity of the geometrical stress concentrators being schematised as shown in Figs 4a to 4b was determined numerically by modelling steel wires having length equal to 100 mm (Fig. 4d). As reported in Ref. [26, 31], the most common chemical composition of the high-strength steels used to make wires is as follows: C(0.85~0.90%), Si(0.12~0.32%), Mn(0.60~0.90%), Cr(0.10~0.25%), S, and Cu. Accordingly, Young's Modulus, E, and Poisson's ratio, ν, were taken equal to 210 GPa and to 0.3, respectively [9].

Three-dimensional Finite Element (FE) analyses of steel wires containing pits and cracks were performed using commercial software ANSYS®, where the axially loaded cables were modelled by employing 10-node tetrahedral solid elements (SOLID92). For all the types of stress concentrators being considered, the mesh density in the critical regions was increased gradually until convergence occurred. As an example, Fig. 4d shows a typical FE model employed in this work to determine the relevant stress distributions in a steel wire containing a hemispherical pit.

As to the results from the numerical stress analysis exercise, it is important to point out here that in the hemispherical pits the maximum stress was seen to be on the wire surface at the edge of the pit mouth (Fig. 4b). In contrast, in the presence of semi-ellipsoidal pits, the maximum stress was calculated to be invariably at the bottom of the cavities (Fig. 4a).

The final aspect that is important to quantify in the present section is the scatter index characterising the population of experimental results summarised in Tables 3, 4 and 5. To this end, the fatigue data being collected from the technical literature were post-processed in terms of nominal gross stress range, $\Delta\sigma_{nom}$, under the hypothesis of a log-normal distribution of the number of cycles to failure for each stress range level and assuming a confidence value equal to 95% [34, 35]. The results from this statistical re-analysis are summarised in the SN log-log diagram plotted in Fig. 5a. This chart shows the range of the nominal gross stress, $\Delta\sigma_{nom}$, against the number of cycles to failure, N_f, with the reported scatter band being delimited by two straight lines corresponding to a probability of survival, P_S, equal to 90% and 10%, respectively. In Fig. 5a T_σ is used to denote the scatter ratio of the endurance limit (in terms of $\Delta\sigma_{nom}$) for 90% and 10% probabilities of survival. The experimental, N_f, vs. estimated, $N_{f,e}$, number of cycles to failure diagram of Fig. 5b shows the accuracy of the P_S=50% curve as estimated in Fig. 5a in predicting the fatigue lifetime of the population of experimental data being considered (Tabs 3 to 5). This diagram makes it evident that the data points fall within an error band of 4. Accordingly, in the next section an error band of 3 will be adopted to quantify the accuracy of both the N-SIF method and the SED approach in estimating the fatigue strength of metallic wires containing corrosion pits and cracks.

4. Results and discussions

The SED method was devised by our colleague Paolo Lazzarin at the beginning of the 2000s to overcome some intrinsic shortcomings characterising the N-SIF approach [19]. In particular, the trickiest aspect associated with the in-field usage of this design methodology is that, according to definitions (1) and (2), N-SIFs are measured in units that vary as the notch opening angle, 2α, varies. As far as the notch fatigue problem is concerned, this implies that, given the material, the results obtained for a specific value of 2α cannot be used to quantify the detrimental effect of stress concentrators having a different value of the notch opening

angle. In addition, the N-SIF approach requires very refined mesh for its application and this is also a drawback for complex structures.

In spite of these intrinsic limitations, the N-SIF approach is well-known for being highly accurate [13], so that, initially, the results summarised in Tables 3 to 5 were attempted to be re-analysed according to this powerful design methodology. To this end, the N-SIFs for pitted and cracked steel wires were determined both by running numerical simulations and by using analytical solutions. The values for r_0, ρ, 2α and λ_1 being used to implement this hybrid strategy are listed in Tab. 6.

The experimental results selected from the technical literature and generated by testing both hemispherical and semi-elliptical notch-like pits were re-analysed under the hypothesis of a log-normal distribution of the number of cycles to failure for each N-SIF range level, with this being done by setting the confidence level invariably equal to 95% [34, 35]. The results from the statistical re-analyses are summarised in the log-log chart of Figs 6a and 6b. The scatter bands seen in these diagrams were calculated for a probability of survival, P_S, equal to 10% and 90%, with their width being quantified by using index $T_{\Delta K}$. This index was determined by calculating the scatter ratio of the endurance limit (in terms of N-SIF range) for 90% and 10% probabilities of survival. As to the semi-elliptical pits being considered in Fig. 6b, since they were characterised by different values not only of the radius, but also of the depth, the associated opening angles were then different. This explains the reason why the experimental results generated by testing semi-elliptical pits were re-analysed in terms of the ratio $\Delta K_1/r_0^{1-\lambda_1}$ and not just in terms of the N-SIF range as done for the hemispherical pits (Fig. 6a).

Turning to wires containing superficial cracks, the associated N-SIF range, ΔK_1, was estimated by taking full advantage of Murakami's formula [36]:

$$\Delta K_1 = 0.65 \cdot \Delta\sigma_{nom} \cdot \sqrt{\pi\sqrt{area}} \tag{14}$$

where $\Delta\sigma_{nom}$ is the nominal gross stress range, and $\sqrt{area}$ is the square root of the area of the crack perpendicular to the loading direction.

The statistical re-analysis of the considered fatigue results was performed again by taking the confidence level equal to 95% and by assuming, for each N-SIF range level, a log-normal distribution of the number of cycles to failure [34, 35]. As far as cracked wires are concerned, Fig. 6c plots, together with the resulting scatter index $T_{\Delta K}$, the relationship between N-SIF range and number of cycles to failure, N_f.

The diagrams reported in Fig. 6 make it evident that, when re-analysed in terms of N-SIF range, the fatigue data falls within relatively narrow scatter bands, with this holding true independently of the type of geometrical defect being considered. In particular, the scatter indices for steel wires with hemispherical pits, semi-elliptical pits, and semi-elliptical cracks were calculated to be equal to 1.541, 2.578, and 1.494, respectively.

As done with other types of stress concentrators [37], also for corroded metallic wires containing geometrical defects it is possible to establish, in a log-log schematisation, a linear relationship between N-SIF range and fatigue lifetime, N_f. Therefore, by using the standard least-squares regression method, it was straightforward to obtain for P_S=50% the following relationships (where N_A was set invariably equal to $2 \cdot 10^6$ cycles to failure):

$$\Delta K_1^k \cdot N_f = \Delta K_{1,A}^k \cdot N_A \qquad \text{with k=2.6 and } \Delta K_{1,A}=336 \text{ MPa}\cdot\text{mm}^{0.477} \tag{15}$$

for hemispherical pits,

$$\left(\frac{\Delta K_1}{\lambda_0^{1-\lambda_1}}\right)^k \cdot N_f = \left(\frac{\Delta K_{1,A}}{\lambda_0^{1-\lambda_1}}\right)^k \cdot N_A \qquad \text{with k=2.9 and } \frac{\Delta K_{1,A}}{\lambda_0^{1-\lambda_1}} = 708 \text{ MPa} \tag{16}$$

for semi-elliptical pits and

$$\Delta K_1^k \cdot N_f = \Delta K_{1,A}^k \cdot N_A \quad \text{with k=2.1 and } \Delta K_{1,A}=99 \text{ MPa}\cdot\text{mm}^{0.5} \tag{17}$$

for semi-elliptical cracks.

Since the units of the stress quantities used in the three charts of Fig. 6 are different, the obtained estimates were plotted together in the experimental, N_f, vs. estimated, $N_{f,e}$, number of cycles to failure diagram of Fig. 7, with this being done to assess the overall accuracy of the N-SIF approach in estimating fatigue damage in pitted/cracked wires. This chart was built by predicting the fatigue lifetime of the pitted/cracked cables under investigation (Tabs 3 to 5) via Eqs (15) to (17) that refer to a probability of survival equal to 50%. The N_f vs. $N_{f,e}$ diagram of Fig. 7 confirms that the use of the N-SIF approach resulted in estimates mainly falling within an error band of 3, i.e. in a level of accuracy higher than the one which was obtained by using the nominal stress approach (Fig. 5b).

As mentioned earlier, while these relationships can directly be employed to assess fatigue damage in corroded/cracked metallic wires, their in-field usage is not at all straightforward. This is due to the fact that, according to the way they are defined, the units of the N-SIFs depend on the value of the notch opening angle. Even if the N-SIF approach is well-known for being very accurate, this aspect makes it difficult for this design methodology to be used in situations of practical interest. All these limitations can be overcome by using the SED approach which allows very coarse meshes to be employed to perform the stress/strain analyses being required for its in-field usage.

Thanks to its unique features, the SED method is a simple and effective tool suitable for performing the fatigue assessment of notched/cracked components. The key advantage over the other existing methods is that the averaged SED can be estimated from standard linear-elastic FE models by directly post-processing the nodal displacements, with the calculated value being independent of the mesh size. In particular, the SED range averaged in a volume, V, can be calculated by simply dividing by V the total energy determined by considering the strain energy, ΔW_{Fi}, associated with any FE element contained in the volume itself, i.e.:

$$\Delta\overline{W} = \frac{\sum_V \Delta\overline{W}_{Fi}}{V} \tag{18}$$

In the SED approach, the control radius, which can directly be determined according to either Eq. (9) or Eq. (10), is a fatigue property which is different for different materials and different load ratios. In other words, given the material and the load ratio, its value does not depend on the profile of the geometrical feature being assessed.

As far as metallic wires are concerned, the threshold value of the stress intensity factor range can be estimated for load ratios larger than zero according to the following empirical expression [38, 39]:

$$\Delta K_{th} = 5.54 - 3.43 \cdot R \ [\text{MPa}\cdot\text{m}^{1/2}] \tag{19}$$

Further, by post-processing the experimental results generated by Liu, Song and Liu [40], it is possible to derive a fatigue curve suitable for designing against fatigue high-strength steel cables having, at $N_A=2\cdot10^6$ cycles to failure, endurance limit, $\Delta\sigma_A$, equal to 256 MPa (for $P_S=50\%$ and $R>0.4$).

By observing that, in situations of practical interest, high-strength steel wires are subjected to axial load histories characterised by large values of the load ratio (typically, R=0.5) [1, 9], a reference value for the control the radius, R_o, can then be estimated according to Eq. (9) as follows:

$$R_0 = \left(\frac{\sqrt{2e_1}\cdot\Delta K_{1,A}}{\Delta\sigma_A}\right)^{\frac{1}{1-\lambda_1}} = \left[\frac{\sqrt{2\cdot0.133}\cdot(5.54-3.43\cdot0.5)\cdot1000^{0.5}}{256}\right]^{\frac{1}{1-0.5}} = 0.06 \text{ mm} \tag{20}$$

This value of the reference radius is well aligned with the values previously derived from other high-strength materials as discussed in Refs [22, 41].

Having estimated a reference value for R_o, the experimental results summarised in Tables 3 to 5 were then re-analysed to determine the corresponding ranges of the averaged SED. In particular, the values of $\Delta\overline{W}$ at the hot-spots (Figs 4a, 4b and 4c) were determined from the

linear-elastic FE models being solved (see Section 3 and Fig. 4d) as well as by taking full advantage of the analytical relationships briefly summarized in Section 2 [22, 41]. The chart of Fig. 8 plots the error that was made by estimating the averaged SED analytically versus the opening angle, 2α, with the error being calculated as:

$$\text{Error} = \frac{\Delta\overline{W}_{\text{Analytical}} - \Delta\overline{W}_{\text{FEM}}}{\Delta\overline{W}_{\text{FEM}}} \cdot 100\ [\%] \tag{21}$$

In definition (21) $\Delta\overline{W}_{\text{Analytical}}$ and $\Delta\overline{W}_{\text{FEM}}$ are, obviously, the averaged SED ranges determined analytically and numerically, respectively. The chart reported in Fig. 8 makes it evident that the use of the analytical solutions briefly recalled in Section 2 resulted in estimates falling within an error interval of ±20%. This level of accuracy is certainly satisfactory especially in light of the fact that these relationships were derived by considering ideal notch shapes and not the specific stress raisers shown in Fig. 4. Fig. 8 then suggests that, while the standard analytical solutions can be used for a rapid estimation of the averaged SED in pitted/cracked wires, attention must be paid in situations of practical interest because these equations return estimates that tend to be slightly non-conservative.

Turning to the fatigue strength problem, the chart of Fig. 9a summarises the experimental results listed in Tables 3 to 5 in terms of numerical value of the averaged SED range, $\Delta\overline{W}$. This diagram makes it evident that, as expected, the relationship between $\Delta\overline{W}$ and N_f can obviously be described (in a log-log representation) by using a simple linear relationship. Thus, a convenient expressions for a reference $\Delta\overline{W}$ vs. N_f curve suitable for designing pitted/cracked steel wires against fatigue were derived via the least-squares method (with $N_A=2\cdot10^6$ cycles to failure), obtaining:

$$\Delta\overline{W}^k \cdot N_f = \Delta\overline{W}_A^k \cdot N_A \text{ with } k=1.5 \text{ and } \Delta\overline{W}_A^k = 0.214\ \text{N}\cdot\text{mm/mm}^3 \tag{22}$$

for a probability of survival, P_S, equal to 50% and

$$\Delta\bar{W}^{k} \cdot N_f = \Delta\bar{W}_A^{k} \cdot N_A \text{ with } k=1.5 \text{ and } \Delta\bar{W}_A^{k} = 0.109 \text{ N·mm/mm}^3 \quad (23)$$

for P_S=90%. It is worth pointing out here that, also in this case, the scatter band seen in Fig. 9a was built by re-analysing the fatigue results under the hypothesis of a log-normal distribution of the number of cycles to failure for each $\Delta\bar{W}$ level, with this being done by setting the confidence level invariably equal to 95% [34, 35].

To quantify the accuracy of the SED approach in estimating the fatigue lifetime of pitted/cracked metallic wires, the predictions being made were then re-plotted in the experimental, N_f, vs. estimated, $N_{f,e}$, number of cycles to failure diagram reported in Fig. 9b. This chart was built by using Eq. (22) - that refers to P_S=50% - to predict the number of cycles to failure for any experimental result being considered (see Tabs 3 to 5). The N_f vs. $N_{f,e}$ diagram of Fig. 9a confirms that the use of the SED approach resulted in estimates mainly falling within an error band of 3. In other words, Fig. 9a makes it evident that the SED approach allowed us to reach the same level of accuracy as the one that was obtained by using the N-SIF method (Fig. 7), the advantage being that the SED approach allows fatigue damage to be estimated by using the same reference design curve independently of the value of the notch opening angle. Another computational advantage is the possibility of using coarse meshes in contrast to the N-SIF approach which requires very refined meshes in the vicinity of the geometrical hot-spots being assessed.

5. Conclusions

The present paper deals with the estimation of fatigue damage in high-strength steel wires weakened by corrosion pits and cracks. All the re-analyses discussed in the previous sections were based on a large number of experimental results that were collected from the literature by carrying out a systematic data-mining exercise [26-33].

As far as pits are concerned, according to the available technical literature [3-8], the associated values of the N-SIFs as well as of the averaged SED were determined numerically (using

commercial software ANSYS®) by modelling them as semi-ellipsoidal or as hemispherical three-dimensional notches. Further, the values of the averaged SED were also attempted to be estimated by using those analytical solutions that were originally derived by considering standard, ideal notch shapes [22-24].

Turning to wires containing semi-elliptical cracks, the corresponding N-SIFs were determined using the well-known formula proposed by Murakami [36]. In contrast, the associated values of the averaged SED were determined not only analytically, but also numerically by modelling the idealised notch shapes shown in Figs 4a and 4b.

The research work being summarised in the present paper allowed us to draw the conclusions listed in the bullet points that are reported in what follows.

- The N-SIF approach can successfully be used also to assess fatigue damage in pitted/cracked high-strength metallic wires (Fig. 6).
- The use of the N-SIF method in situations of practical interest is somehow limited by the fact that different reference design curves must be employed as type and shape of the stress concentrator being assessed change. In addition, a very fine mesh is necessary for the application of this approach and this is a clear limitation in case of 3D structures or very complex geometries.
- For rapid calculations, the averaged SED range damaging pitted/cracked metallic wires during in-service operations can be quantified by using those analytical solutions that were derived by considering standard notches. However, attention must be paid because the values being determined according to this simplified procedure are seen to be slightly non-conservative (Fig. 8).
- As far as pitted/cracked high-strength steel wires are concerned, the SED approach can be applied (also with coarse meshes) in the presence of large values of the load ratio (i.e., $R \approx 0.5$) by setting the control radius, R_0, equal to 0.06 mm, Eq. (20).
- The SED approach is seen to be successful in modelling the fatigue strength of pitted/cracked high-strength metallic cables (Fig. 9).

- The use of nominal stresses is seen to result in estimates falling within an error band of 4. In contrast, both the N-SIF and the SED approach allow a higher level of accuracy to be reached, with the obtained estimates falling mainly within an error band of 3.

Acknowledgements

This research is supported by National Natural Science Foundation of China under Grant No. 51708305, Zhejiang Provincial Natural Science Foundation of China under Grant No. LQ17E080005 and K. C. Wong Magna Fund in Ningbo University.

References

[1] Nakamura S, Suzumura K, Tarui T. Mechanical properties and remaining strength of corroded bridge wires. Struct Eng Int 2004;14(1):50-54.

[2] Anon. Standard Guide for Examination and Evaluation of Pitting Corrosion. ASTM International, ASTM G46-94(2018), West Conshohocken, PA; 2018.

[3] Eubank RA. Stress concentration due to a hemispherical pit at a free surface. J Appl Mech 1954;21:57-62.

[4] Chen GS, Wan K, Gao M, Wei RP, Flournoy TH. Transition from pitting to fatigue crack growth—modeling of corrosion fatigue crack nucleation in a 2024-T3 aluminum alloy. Mater Sci Eng A Struct Mater 1996;219(1):126-132.

[5] Kondo Y. Prediction of Fatigue Crack Initiation Life Based on Pit Growth. Corrosion 1989;45(1):7-11.

[6] Cerit M, Genel K, Eksi S. Numerical investigation on stress concentration of corrosion pit. Eng Fail Anal 2009;16(7):2467-2472.

[7] Turnbull A, Horner DA, Connolly BJ. Challenges in modelling the evolution of stress corrosion cracks from pits. Eng Fract Mech 2009;76(5):633-640.

[8] Turnbull A, Wright L, Crocker L. New insight into the pit-to-crack transition from finite element analysis of the stress and strain distribution around a corrosion pit. Corros Sci 2010;52(4):1492-1498.

[9] Jie Z, Susmel L. High-strength steel wires containing corrosion pits: stress analysis and critical distance based fatigue life estimation. Fatigue Fract Eng Mater Struct. 2019;1–18. https://doi.org/10.1111/ffe.13157.

[10] Susmel L. The theory of critical distances: a review of its applications in fatigue. Eng Fract Mech 2008;75(7):1706-1724.

[11] Taylor D. The theory of critical distances. Eng Fract Mech 2008;75(7):1696-1705.

[12] Atzori B, Lazzarin P, Meneghetti G. Fatigue strength assessment of welded joints: From the integration of Paris' law to a synthesis based on the notch stress intensity factors of the uncracked geometries. Eng Fract Mech 2008;75(3-4):364-378.

[13] Lazzarin P, Tovo R. A notch intensity factor approach to the stress analysis of welds. Fatigue Fract Eng M 1998;21(9):1089-1103.

[14] Lazzarin P, Berto F, Gomez FJ, Zappalorto M. Some advantages derived from the use of the strain energy density over a control volume in fatigue strength assessments of welded joints. Int J Fatigue 2008;30(8):1345-1357.

[15] Song W, Liu X, Razavi SMJ. Fatigue assessment of steel load-carrying cruciform welded joints by means of local approaches. Fatigue Fract Eng M 2018;41(12):2598-2613.

[16] Meneghetti G. The peak stress method applied to fatigue assessments of steel and aluminium fillet-welded joints subjected to mode I loading. Fatigue Fract Eng M 2008;31(5):346-369.

[17] Meneghetti G, Lazzarin P. The peak stress method for fatigue strength assessment of welded joints with weld toe or weld root failures. Weld World 2011;55(7-8):22-29.

[18] Lazzarin P, Berto F, Zappalorto M. Rapid calculations of notch stress intensity factors based on averaged strain energy density from coarse meshes: theoretical bases and applications. Int J Fatigue 2010;32(10):1559-1567.

[19] Lazzarin P, Zambardi R. A finite-volume-energy based approach to predict the static and fatigue behaviour of components with sharp V-shaped notches. Int J Fracture 2001;112(3):275-298.

[20] Lazzarin P, Tovo R. A unified approach to the evaluation of linear elastic stress fields in the neighborhood of cracks and notches. Int J Fracture 1996;78(1):3-19.

[21] Ellyin, F. Fatigue Damage, Crack Growth and Life Prediction. Chapman & Hall, Thompson Press Ltd, New Delhi, India, 1997.

[22] Berto F., Lazzarin P., Recent developments in brittle and quasi-brittle failure assessment of engineering materials by means of local approaches . Mater. Sci. Eng. R 2014;75:1-48.

[23] Razavi SMJ, Ferro P, Berto F, Torgersen J. Fatigue strength of blunt V-notched specimens produced by selective laser melting of Ti-6Al-4V. Theor Appl Fract Mec 2018;97:376-384.

[24] Lazzarin P, Berto F. Some expressions for the strain energy in a finite volume surrounding the root of blunt V-notches. Int J Fracture 2005;135(1-4):161-185.

[25] Filippi S, Lazzarin P. Distributions of the elastic principal stress due to notches in finite size plates and rounded bars uniaxially loaded. Int J Fatigue 2004;26(4):377-391.

[26] Jiang C, Wu C, Jiang X. Experimental study on fatigue performance of corroded high-strength steel wires used in bridges. Constr Build Mater 2018;187:681-690.

[27] Lan CM. Study on life-cycle safety assessment methods for parallel wire stay cable. School of Civil Engineering, Harbin Institute of Technology, Harbin, China, 2009 - http://cdmd.cnki.com.cn/Article/CDMD-10213-2009292188.htm

[28] Zheng XL. Research on the fatigue performance of corroded steel wire and evaluation method of fatigue reliability for bridge cables. College of Civil Engineering and Architecture, Zhejiang University, Hangzhou, China, 2018. - http://cdmd.cnki.com.cn/Article/CDMD-10335-1018244275.htm

[29] Hou XD. Experimental study and numerical analysis on fatigue strength of parallel wire based on corrosion classification. College of Civil Engineering, Nanjing Forestry University, Nanjing, China, 2015 - http://cdmd.cnki.com.cn/Article/CDMD-10298-1015809242.htm

[30] Sun CZ. Assessment of safety capability and fatigue life of corroded cable for cable-supported Bridge. College of Civil Engineering, Southeast University, Nanjing, China, 2013 - http://www.wanfangdata.com.cn/details/detail.do?_type=degree&id=Y2511929

[31] Llorca J, Sánchez Gálvez V. Fatigue limit and fatigue life prediction in high strength cold drawn eutectoid steel wires. Fatigue Fract Eng M 1989;12(1):31-45.

[32] Jiang JH, Ma AB, Weng WF, Fu GH, Zhang YF, Liu GG, Lu FM. Corrosion fatigue performance of pre-split steel wires for high strength bridge cables. Fatigue Fract Eng M 2009;32(9):769-779.

[33] Yan JC. Corrosion of Steel Wire with Corrosion Pit Form Research on the Influence of the Stress Intensity Factor. School of Civil Engineering, Changsha University of Science & Technology, Shangsha, China, 2017 - http://cdmd.cnki.com.cn/Article/CDMD-10536-1018249198.htm

[34] Spindel JE, Haibach E. Some considerations in the statistical determination of the shape of S-N cruves. In: Statistical Analysis of Fatigue Data, ASTM STP 744 (Edited by Little, R. E. and Ekvall, J. C.), pp. 89–113, 1981.

[35] Al Zamzami, I., Susmel, L. On the accuracy of nominal, structural, and local stress based approaches in designing aluminium welded joints against fatigue. Int J Fatigue 101 (2), pp. 137-158, 2017.

[36] Lambrighs K, Wevers M, Verlinden B, Verpoest I. A fracture mechanics approach to fatigue of heavily drawn steel wires. Procedia Eng 2011;10:3259-3266.

[37] Lazzarin P, Livieri P. Notch stress intensity factors and fatigue strength of aluminium and steel welded joints. Int J Fatigue 2001;23(3):225-232.

[38] Llorca J, Sánchez-Gálvez V. Fatigue threshold determination in high strength cold drawn eutectoid steel wires. Eng Frac Mech 1987;26(6);869-882.

[39] Petit J, Sarrazin-Baudoux C, Lorenzi F. Fatigue crack propagation in thin wires of ultra high strength steels. Procedia Engineering 2010;2(1):2317-2326.

[40] Li XL, Song XH, Liu YQ. Investigation on fatigue reliability of high strength galvanized steel wires. China Civil Eng J 1995;28(2):36-43.

[41] Berto F., Lazzarin P. A review of the volume-based strain energy density approach applied to V-notches and welded structures. Theor. Appl. Fract. Mech. 2009; 52 (3): 183-194.

Lists of Captions

Tables

2α *[deg]*	λ_1	λ_2
0	0.5	0.5
15	0.5002	0.5453
30	0.5014	0.5982
45	0.505	0.6597
60	0.5122	0.7309
90	0.5445	0.9085
120	0.6157	1.1489
135	0.6736	1.3021
150	0.752	1.4858
160	0.8187	1.6305
170	0.9	1.7989

Table 1. Williams' eigenvalues,

2α *[deg]*	$\tilde{\omega}_1$	$F(2\alpha)$
0	1	0.785
30	1.034	0.6917
45	1.014	0.6692
60	0.97	0.662
90	0.81	0.7049
120	0.57	0.8779
135	0.432	1.0717
150	0.288	1.4417

Table 2. Constants for the analytical calculation of the SED for blunt notches.

Code	Δσ [MPa]	R	N_f [Cycles]	d [mm]	*l* [mm]	w [mm]	*D* [mm]	σ_{UTS} [MPa]
H1	290	0.5	348000	0.364	0.728	0.728	4.916	1570
H2	360		214000					
H3	500		91500					
H4	640		48300					
A-1	520	0.4	162711	0.18	0.36	0.36	6.84	1835
A-2	450		220664					
A-3	360		464954					
B-1	520	0.4	132464	0.26	0.52	0.52	6.7	1835
B-2	450		185447					
B-3	360		366536					
C-1	520	0.4	73560	0.39	0.78	0.78	6.6	1835
C-2	450		123274					
C-3	360		230367					
C-4	270		1E+06					
D-1	520	0.4	59111	0.54	1.08	1.08	6.4	1835
D-2	450		103675					
D-3	360		163443					
D-4	270		586464					
E-1	520	0.4	57457	0.6	1.2	1.2	6.36	1835
E-2	450		83697					
E-3	360		159810					
E-4	270		510750					
F-1	520	0.4	47727	0.68	1.36	1.36	6.24	1835
F-2	450		67622					
F-3	360		127807					
F-4	270		306577					

Table 3. Summary of the fatigue results generated by testing wire weakened by hemispherical pits [26, 27].

Code	Δσ [MPa]	R	N_f [Cycles]	d [mm]	*l* [mm]	*D* [mm]	σ_{UTS} [MPa]
S1	360	0.5	359857	0.246	0.89	5	1570
S2	440		168571				
S3	520		104861				
S4	360	0.4	472341	0.184	4.06	7	1770
S5	450		217172				
S6	600		85446				
S7	750		51900				
S8	360	0.4	263066	0.403	9.93	7	1770
S9	450		140634				
S10	600		73688				
S11	750		37848				
A1-1-1	312	0.55	141177	0.5	8	5	1570
A1-1-2	392		75599				
A1-1-3	500		25008				
A1-1-4	628		14247				
A1-2-1	330	0.44	75056	0.5	8	5	1570
A1-2-2	521		23780				
A1-2-3	672		17900				
A1-2-4	840		9921				
A1-3-1	520	0.35	385115	0.5	8	5	1570
A1-3-2	640		135483				
A1-3-3	840		66102				
A1-3-4	1040		26089				
A2-1	330	0.44	74268	0.5	3	5	1570
A2-2	521		38124				
A2-3	672		19518				
A2-4	840		10037				
A3-1	330	0.44	78318	0.5	5	5	1570
A3-2	521		46700				
A3-3	672		25597				
A3-4	840		11351				
A4-1	330	0.44	57669	0.6	5	5	1570
A4-2	521		25279				
A4-3	672		11815				
A4-4	840		8597				
A5-1	330	0.44	115798	0.4	5	5	1570
A5-2	521		60300				
A5-3	672		33921				
A5-4	840		24300				

Table 4 (Continued on the next page)

Code	Δσ [MPa]	R	N_f [Cycles]	d [mm]	*l* [mm]	*D* [mm]	σ_{UTS} [MPa]
N1	400	0.667	443812	0.48	3.66	7	1670
N2			417042	0.41	3.28		
N3			452636	0.41	2.88		
N4			451311	0.37	2.84		
N5			536748	0.36	2.86		
N6			451869	0.34	2.54		
N7			422880	0.34	2.16		
N8			513352	0.34	2.3		
N9			416224	0.33	2.18		
N10			589836	0.32	2.46		
N11			450168	0.6	6.26		
N12	500	0.6	206565	0.3	1.86	7	1670
N13			215685	0.53	4.64		
N14			245478	0.47	4.16		
N15			245928	0.46	3.76		
N16			248607	0.37	2.54		
N17			250104	0.3	1.96		

Table 4. Summary of the fatigue results generated by testing wire weakened by semi-elliptical pits [28-30, 33].

Code	$\Delta\sigma$ *[MPa]*	R	N_f *[Cycles]*	a *[mm]*	b *[mm]*	D *[mm]*
M1	690.1	0.061	109810			
M2	578.1	0.069	164120			
M3	387.1	0.52	334620			
M4	490.2	0.52	158590			
M5	527.1	0.18	171450			
M6	583.1	0.49	84780			
M7	346.3	0.66	343380			
M8	400.8	0.34	328080	0.1	1	7
M9	570.4	0.49	92100			
M10	356.5	0.64	376080			
M11	441.8	0.47	253800			
M12	579.3	0.38	133550			
M13	598.4	0.52	103050			
M14	446.9	0.49	194330			
M15	357.8	0.64	270770			

Table 5. Summary of the fatigue results generated by testing wire weakened by semi-elliptical cracks [31, 32].

Code	$\mathbf{r_0}$ *[mm]*	ρ *[mm]*	$\mathbf{2\alpha}$ *[deg]*	λ_1
H1-H4	0.138	0.364		0.523
A	0.068	0.18		0.523
B	0.099	0.26		0.523
C	0.148	0.39	70	0.523
D	0.205	0.54		0.523
E	0.228	0.6		0.523
F	0.258	0.68		0.523
S1-S3	0.254	0.805	97	0.5611
S4-S7	1.723	22.396	165	0.8594
S8-S11	4.12	61.169	168	0.8756
A1	2.068	18.25	157	0.7987
A2	0.617	2.5	121	0.6157
A3	1.133	6.5	142	0.7102
A4	1.102	5.508	135	0.6736
A5	1.177	8.013	149	0.7468
N1	1.493	6.977	131	0.6582
N2	1.358	6.56	133	0.6659
N3	1.15	5.058	127	0.6427
N4	1.166	5.45	131	0.6582
N5	1.176	5.68	133	0.6659
N6	1.031	4.744	130	0.6543
N7	0.825	3.431	123	0.6273
N8	0.898	3.89	126	0.6389
N9	0.843	3.6	125	0.635
N10	1.012	4.728	131	0.6582
N11	2.784	16.328	143	0.7154
N12	0.703	2.883	122	0.6234
N13	1.995	10.155	136	0.6788
N14	1.775	9.205	137	0.6841
N15	1.564	7.683	134	0.6697
N16	0.992	4.359	127	0.6427
N17	0.76	3.201	124	0.6311
M1-M15	-	-	0	0.5

Table 6. Stress analysis parameters for pitted/cracked wires.

Figures

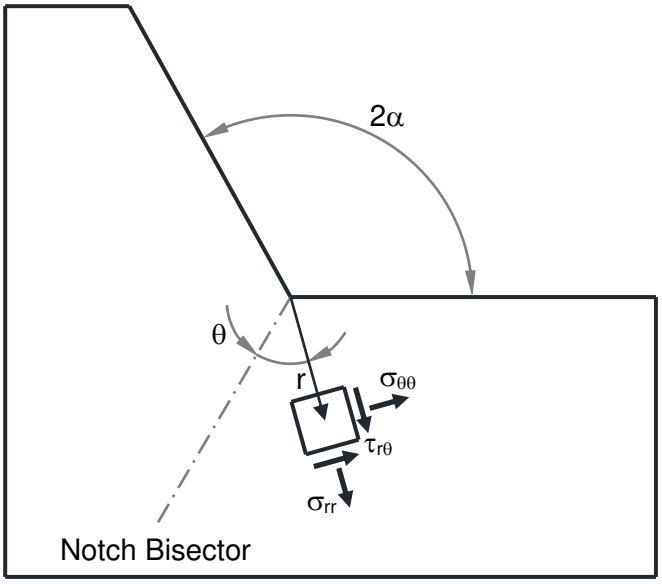

Figure 1. Sharp open notch: local coordinate system and stress components.

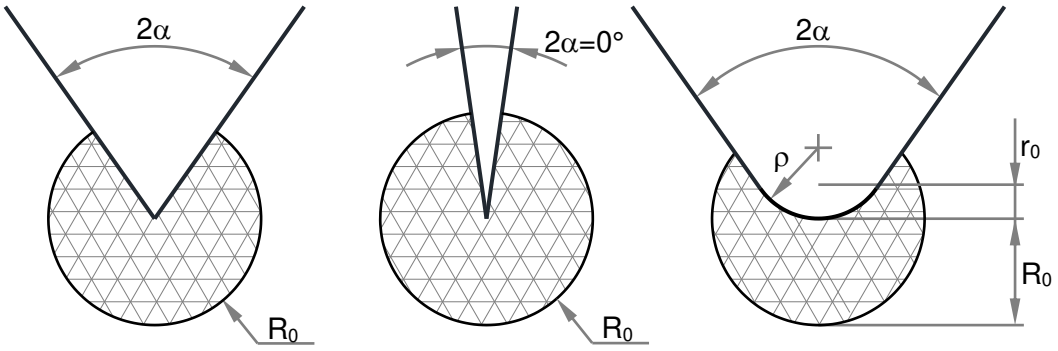

Figure 2. Control volume for a sharp V-notch, a crack and a blunt V-notch.

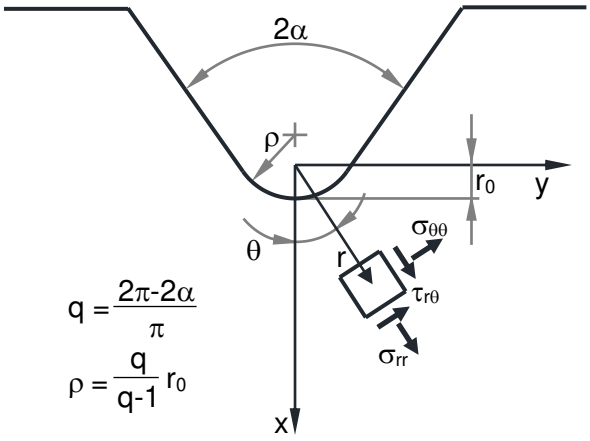

Figure 3. Blunt open notch: coordinate system, stress components and related geometrical quantities.

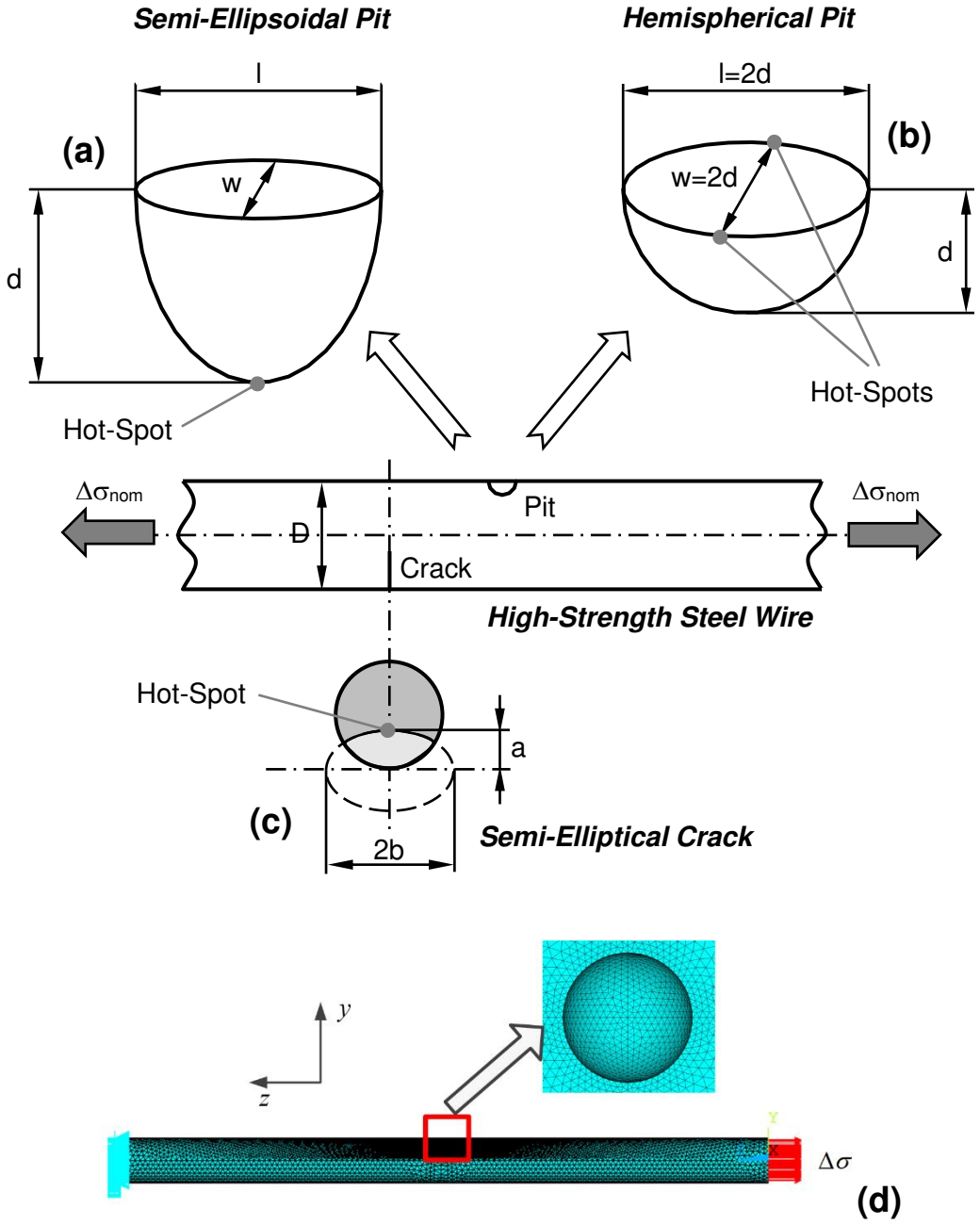

Figure 4. Shapes used to model corrosion pits (a, b), cable weakened by a semi-elliptical crack (c), and example of a FE model of a steel wire containing a hemispherical pit (d).

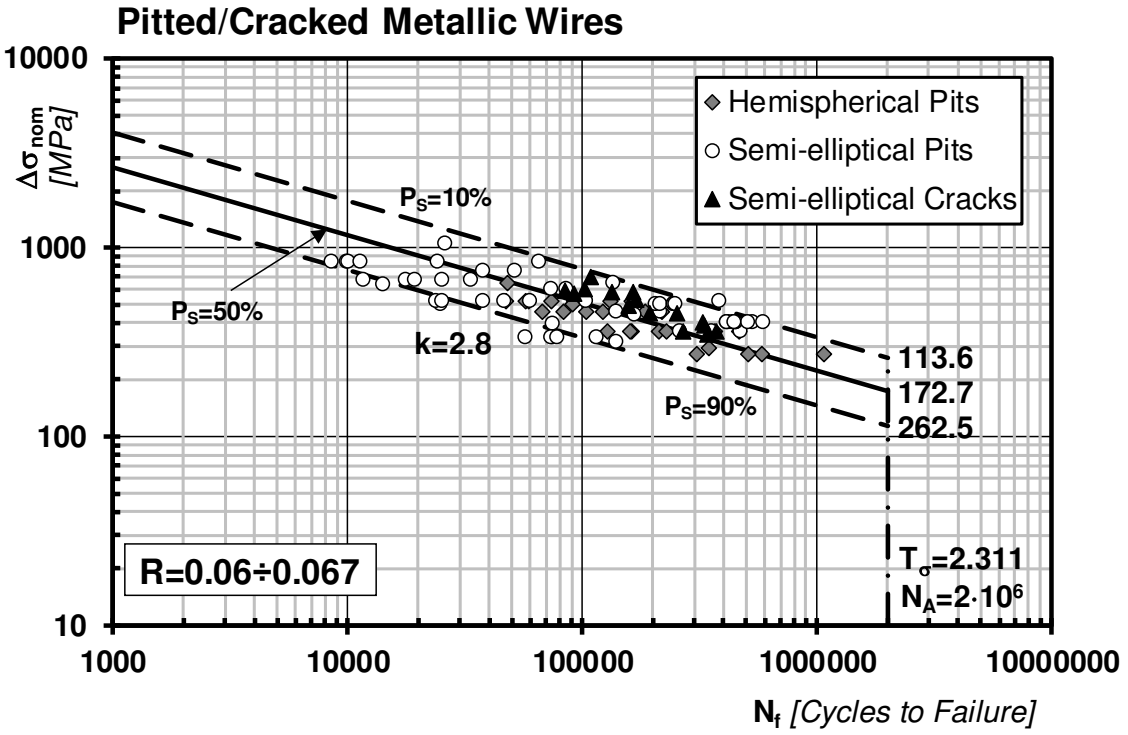

(a)

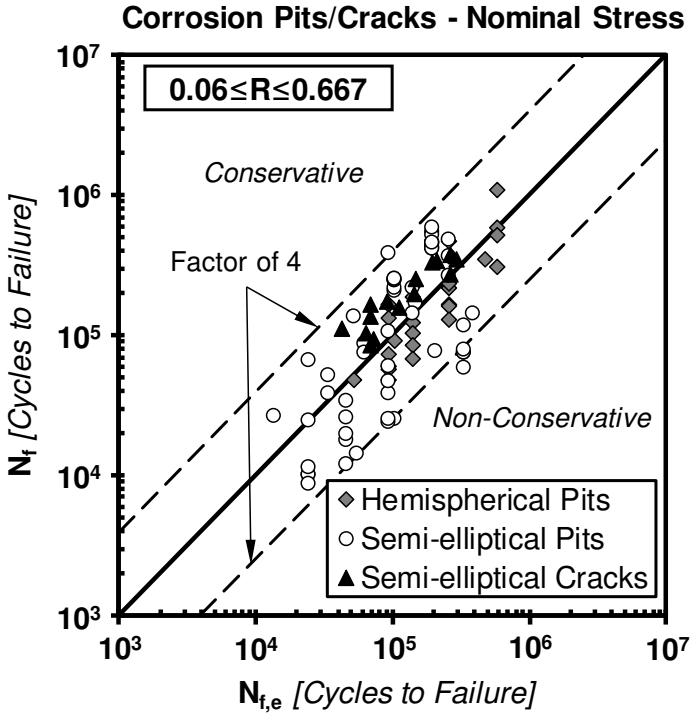

(b)

Figure 5. SN curve statistically determined by re-analysing, in terms of nominal stress range, $\Delta\sigma_{nom}$, the experimental results reported in Tables 3, 4 and 5 (a) and error band of 4 plotted in an experimental, N_f, vs. estimated, $N_{f,e}$, number of cycles to failure diagram (b).

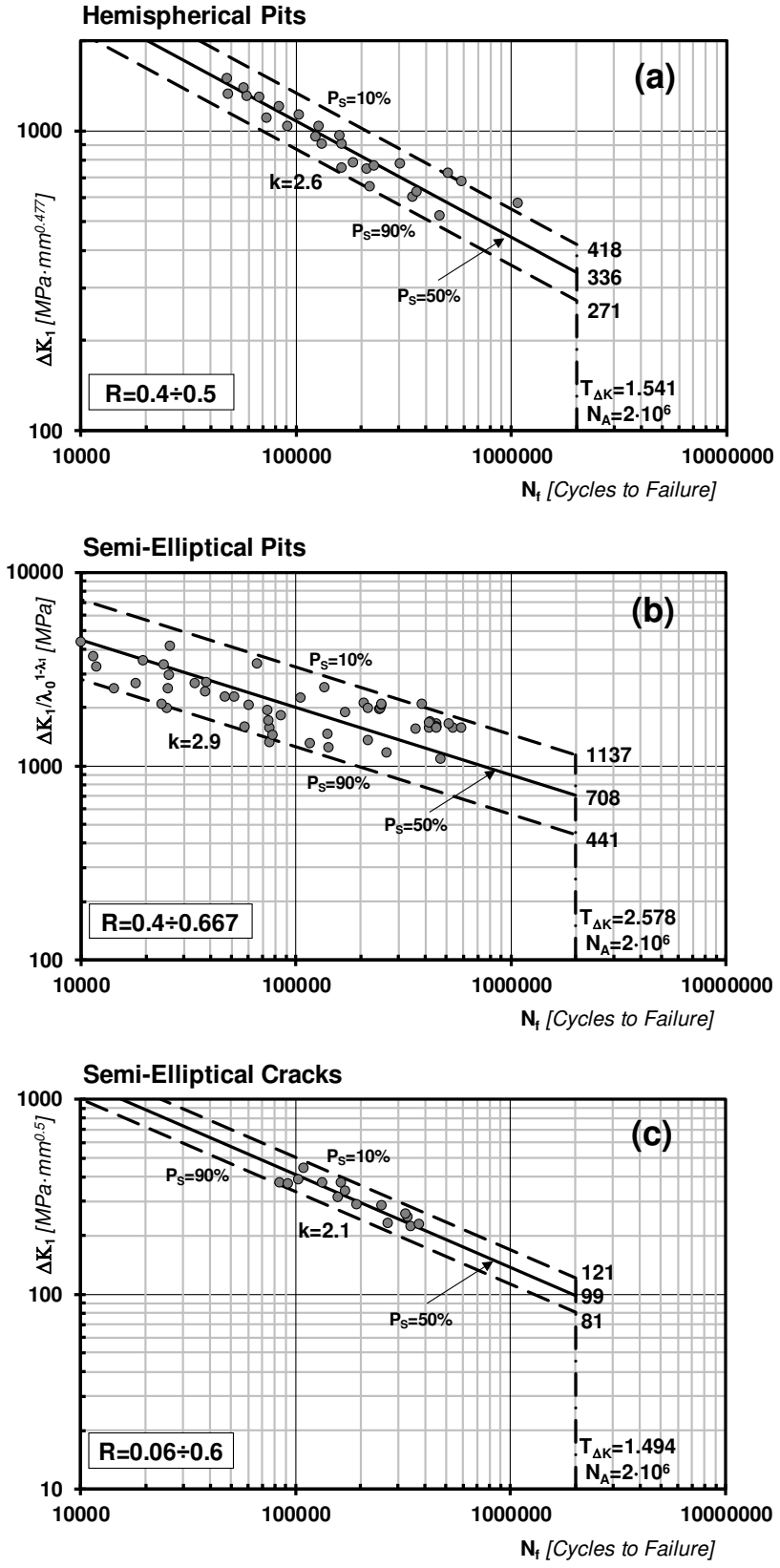

Figure 6. N-SIF approach used to re-analyse the experimental results generated by testing wires containing hemispherical pits (a), semi-elliptical pits (b), and semi-elliptical cracks (c).

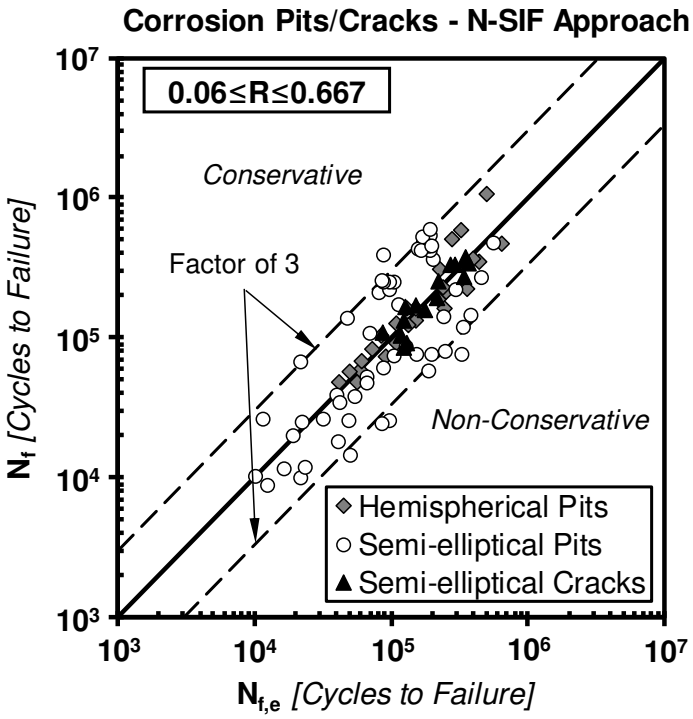

Figure 7. Accuracy of the N-SIF approach summarised in an experimental, N_f, vs. estimated, $N_{f,e}$, number of cycles to failure diagram.

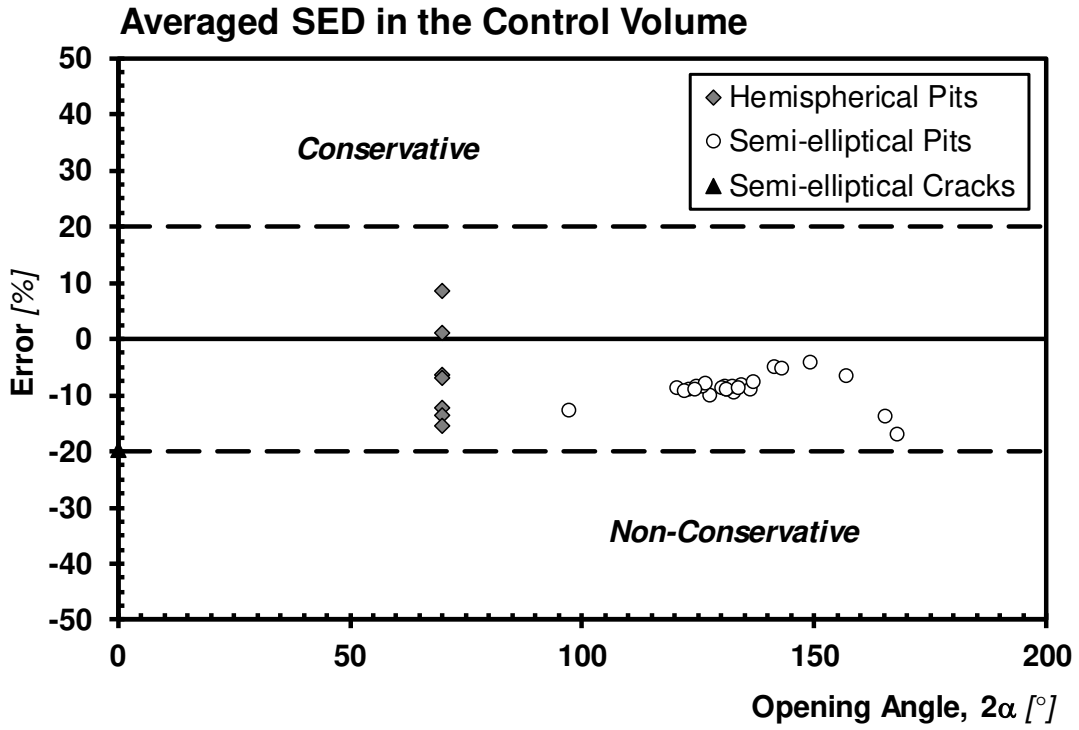

Figure 8. Comparison between averaged SED determined numerically and averaged SED estimated analytically.

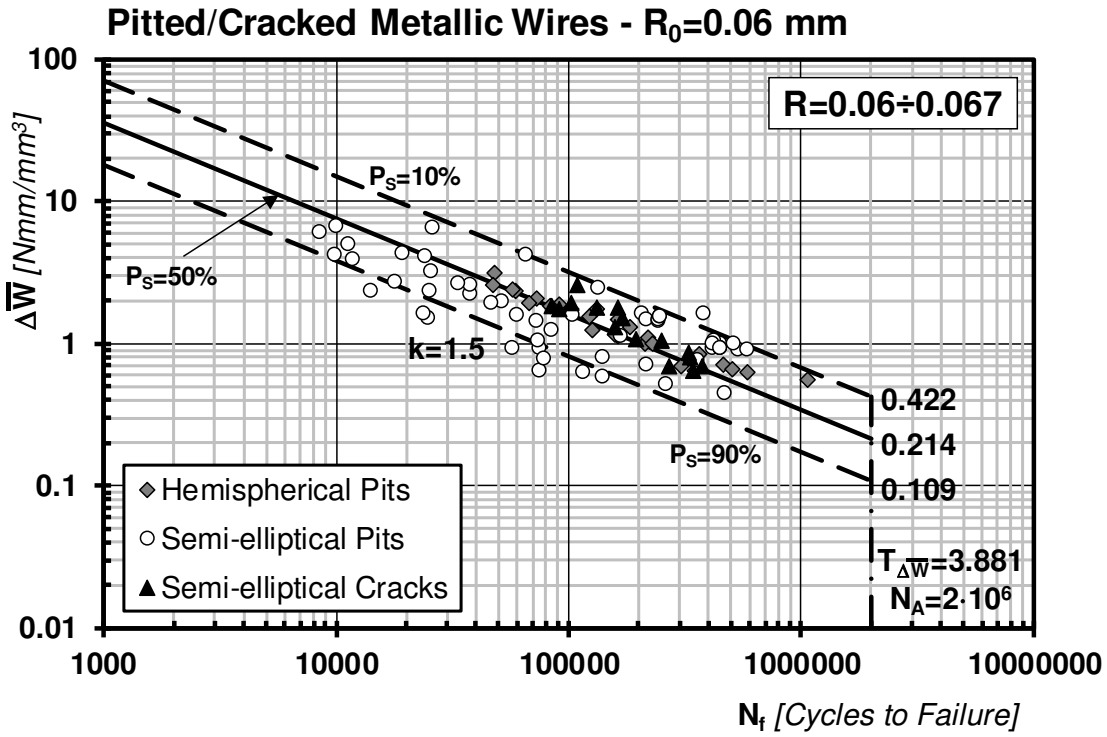

(a)

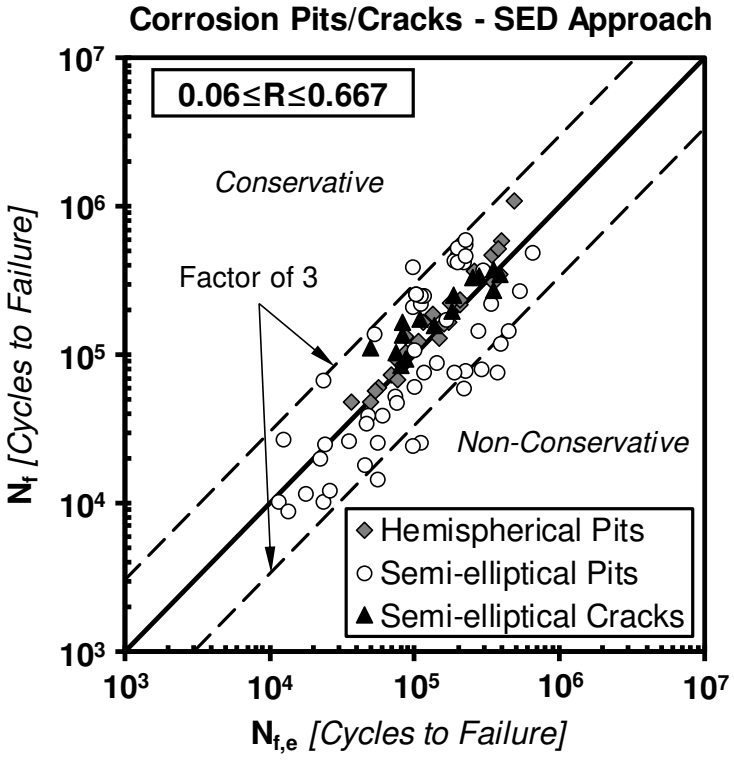

(b)

Figure 9. Fatigue curve statistically determined by re-analysing, in terms of averaged SED range, $\Delta\bar{W}$, the experimental results reported in Tables 3, 4 and 5 (a); accuracy of the SED approach summarised in an experimental, N_f, vs. estimated, $N_{f,e}$, number of cycles to failure diagram. (b).